MIT Libraries | DSpace@MIT

MIT Open Access Articles

A Super-Earth Transiting a Naked-Eye Star

The MIT Faculty has made this article openly available. ***Please share*** how this access benefits you. Your story matters.

Citation: Winn, Joshua N. et al. "A SUPER-EARTH TRANSITING A NAKED-EYE STAR." The Astrophysical Journal 737.1 (2011): L18.

As Published: http://dx.doi.org/10.1088/2041-8205/737/1/l18

Publisher: IOP Publishing

Persistent URL: http://hdl.handle.net/1721.1/71127

Version: Author's final manuscript: final author's manuscript post peer review, without publisher's formatting or copy editing

Terms of use: Creative Commons Attribution-Noncommercial-Share Alike 3.0

Massachusetts Institute of Technology

ACCEPTED VERSION, JULY 6, 2011
Preprint typeset using LaTeX style emulateapj v. 11/10/09

arXiv:1104.5230v3 [astro-ph.EP] 7 Jul 2011

A SUPER-EARTH TRANSITING A NAKED-EYE STAR*

JOSHUA N. WINN[1], JAYMIE M. MATTHEWS[2], REBEKAH I. DAWSON[3], DANIEL FABRYCKY[4,5], MATTHEW J. HOLMAN[3], THOMAS KALLINGER[2,6], RAINER KUSCHNIG[6], DIMITAR SASSELOV[3], DIANA DRAGOMIR[5], DAVID B. GUENTHER[7], ANTHONY F. J. MOFFAT[8], JASON F. ROWE[9], SLAVEK RUCINSKI[10], WERNER W. WEISS[6]

ApJ Letters, in press

ABSTRACT

We have detected transits of the innermost planet "e" orbiting 55 Cnc (V = 6.0), based on two weeks of nearly continuous photometric monitoring with the *MOST* space telescope. The transits occur with the period (0.74 d) and phase that had been predicted by Dawson & Fabrycky, and with the expected duration and depth for the crossing of a Sun-like star by a hot super-Earth. Assuming the star's mass and radius to be $0.963^{+0.051}_{-0.029}\ M_\odot$ and $0.943 \pm 0.010\ R_\odot$, the planet's mass, radius, and mean density are $8.63 \pm 0.35\ M_\oplus$, $2.00 \pm 0.14\ R_\oplus$, and $5.9^{+1.5}_{-1.1}$ g cm^{-3}. The mean density is comparable to that of Earth, despite the greater mass and consequently greater compression of the interior of 55 Cnc e. This suggests a rock-iron composition supplemented by a significant mass of water, gas, or other light elements. Outside of transits, we detected a sinusoidal signal resembling the expected signal due to the changing illuminated phase of the planet, but with a full range (168 ± 70 ppm) too large to be reflected light or thermal emission. This signal has no straightforward interpretation and should be checked with further observations. The host star of 55 Cnc e is brighter than that of any other known transiting planet, which will facilitate future investigations.

Subject headings: planetary systems — planets and satellites: formation, interiors — stars: individual (55 Cnc)

1. INTRODUCTION

Precise Doppler observations have revealed five planets orbiting the nearby G8 V star 55 Cnc (Butler et al. 1997, Marcy et al. 2002, McArthur et al. 2004, Wisdom 2005, Fischer et al. 2008). Only a few other stars are known to host as many planets: HD 10180 (Lovis et al. 2011), Kepler-11 (Lissauer et al. 2011), and the Sun. Among the other reasons why 55 Cnc has attracted attention are the 3:1 resonance between two of its planets (Novak et al. 2003), the existence of an M dwarf companion at a distance of 10^3 AU (Mugrauer et al. 2006), and the unusually low mass and short period of its innermost planet, designated "e".

McArthur et al. (2004) reported a period and minimum mass for 55 Cnc e of 2.8 d and 14 $M_\oplus$, respectively. Those parameters were confirmed by Fischer et al. (2008). More recently, Dawson & Fabrycky (2010) argued that 55 Cnc e had been mischaracterized due to aliasing in the radial-velocity data, and that the true period and minimum mass are 0.74 d and 8 $M_\oplus$.

One implication of the shorter period would be an increased transit probability, from 13% to 25%. The occurrence of transits enhances the importance of an exoplanetary system, because transits can reveal many details about the planet's dimensions, atmosphere, and orbit (see, e.g., Winn 2010).

Fischer et al. (2008) searched for transits in their 11-year photometric record, ruling out transits for planets b (P = 14.7 d) and c (44.3 d). However, the time coverage was not complete enough to rule out transits for planets f (260 d) and d (5200 d), and the precision was insufficient to detect transits of the smallest planet e.

Here, we present space-based photometry of 55 Cnc revealing a transit signal with the characteristics predicted by Dawson & Fabrycky (2010). Section 2 presents the data, and Section 3 presents the light curve analysis, yielding estimates for the mass, radius, and density of the planet. In Section 4 we place 55 Cnc e in the context of the small but growing population of super-Earths with measured masses and radii.

While this manuscript was under review, we learned that Demory et al. (2011) detected a transit of 55 Cnc with the *Spitzer Space Telescope*. We refer the reader to that work for a complementary analysis of the system properties.

2. OBSERVATIONS

We observed 55 Cnc with *MOST* (Microvariability & Oscillations of STars), a Canadian microsatellite equipped with a 15 cm telescope and CCD photometer, capable of short-cadence, long-duration ultraprecise optical photometry of bright stars (Walker et al. 2003, Matthews et al. 2004). *MOST* is in a Sun-synchronous polar orbit 820 km above the terminator with an orbital period of 101 min. Its custom broadband filter covers the visible spectrum (350-700 nm).

We used the Direct Imaging mode, similar to conventional ground-based CCD photometry. The observations were nearly continuous from 2011 February 07-22, except for a few interruptions when cosmic ray hits during passages through the South Atlantic Anomaly resulted in the loss of fine track-

* Based on data from the *MOST* satellite, a Canadian Space Agency mission, jointly operated by Dynacon Inc., the University of Toronto Institute for Aerospace Studies, and the University of British Columbia, with the assistance of the University of Vienna.

[1] Department of Physics, and Kavli Institute for Astrophysics and Space Research, Massachusetts Institute of Technology, Cambridge, MA 02139
[2] Department of Physics and Astronomy, University of British Columbia, 6224 Agricultural Road, Vancouver, BC V6T 1Z1, Canada
[3] Harvard-Smithsonian Center for Astrophysics, 60 Garden St., Cambridge, MA 02138
[4] Hubble Fellow
[5] UCO/Lick Observatory, University of California, Santa Cruz, CA 95064
[6] University of Vienna, Institute for Astronomy, Türkenschanzstrasse 17, A-1180 Vienna, Austria
[7] Department of Astronomy and Physics, Saint Mary's University, Halifax, NS B3H 3C3, Canada
[8] Département de Physique, Université de Montréal, C.P. 6128, Succ. Centre-Ville, Montréal, QC H3C 3J7, Canada
[9] NASA Ames Research Center, Moffett Field, CA 94035
[10] Department of Astronomy & Astrophysics, University of Toronto, 50 St. George Street, Toronto, ON M5S 3H4, Canada

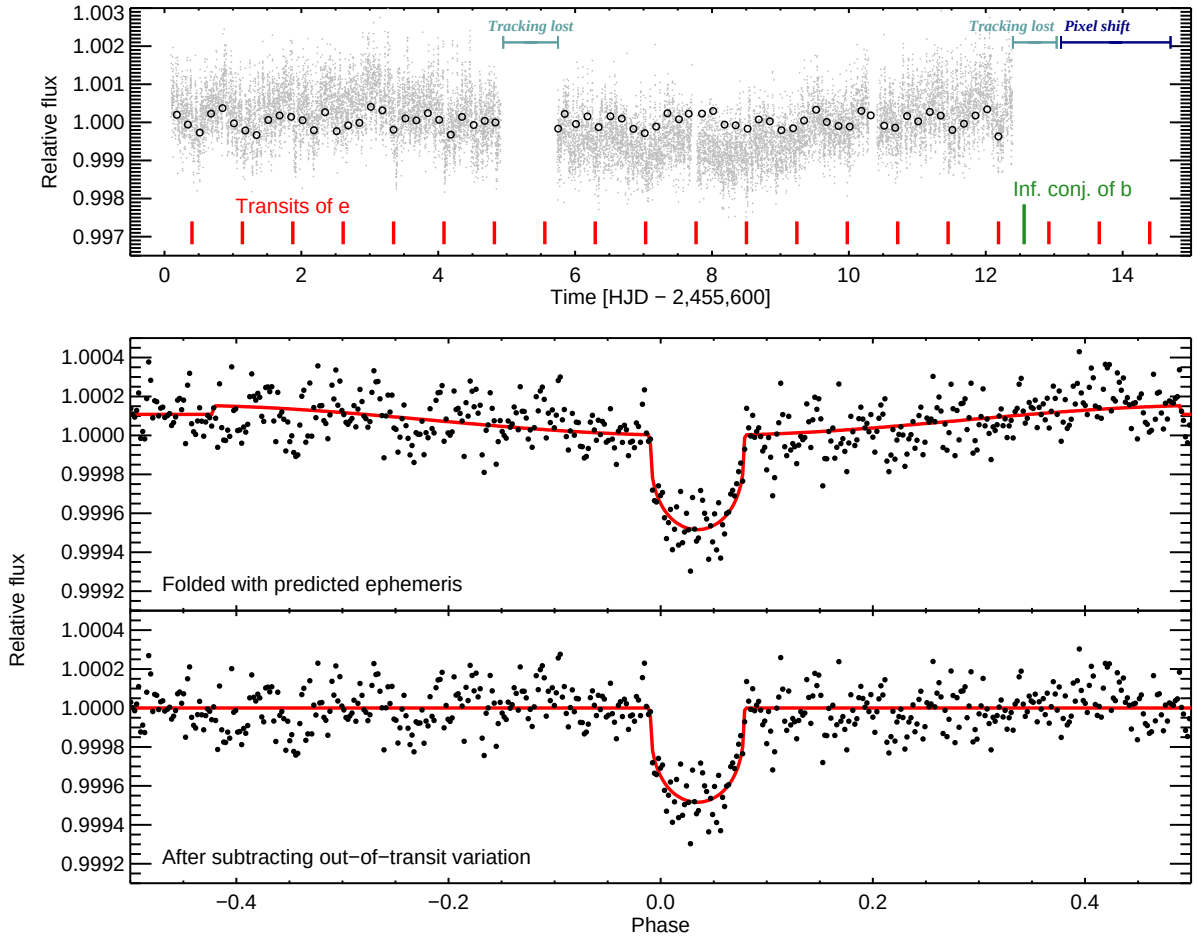

FIG. 1.— *MOST* **photometry of 55 Cnc.** *Upper.*—The time series, after decorrelation (small gray dots) and after further correction with the running averaged background method (large open circles, 0.25 d averages). Vertical bars mark the predicted transit times of planet e, and the inferior conjunction of planet b (which was missed during a failure of fine tracking). *Middle.*—Phased light curve, folded with $P = 0.736540$ d and T_c [HJD] = 2,453,094.6924 (Dawson & Fabrycky 2010) and averaged into 2 min phase bins. The solid curve is the best-fitting model. *Bottom.*—Same, but with the best-fitting model of the out-of-transit variation has been subtracted from the data.

ing. Individual exposures lasted 0.5 s but were downloaded in stacks of 40 for the first 0.6 d, and stacks of 80 for the remaining 14.4 d.

Aperture photometry was performed on the Direct Imaging subraster of the Science CCD. Data affected by cosmic rays, image motion, or other problems were identified and removed. To improve the homogeneity of the data, we omitted data from the first 0.6 d (which had a different effective exposure time) and the final 2.1 d (which suffered from a tracking loss followed by a major shift in image registration). The final time series has 18,373 data points and a time sampling of 43 s outside of the interruptions.

Further processing was needed to remove the familiar periodic artifacts in the time series due to scattered Earthshine. First, the observed magnitude of 55 Cnc was fitted to a linear function of the background level, X position, and Y position, and then this function was subtracted from the observed magnitudes. The Fourier spectrum still had significant peaks at the 14.26 c d^{-1} orbital frequency of the satellite and its harmonics, as well as sidelobes at ± 1 c d^{-1} away from those frequencies (arising from the modulation of the stray light by the Earth's albedo pattern as viewed by the satellite). For this reason, an additional correction was performed with the "running averaged background" method of Rucinski et al. (2004). The data were divided into 5 time intervals, each spanning approximately 32 *MOST* orbits (2.3 d). Within each interval, the data were folded with the satellite's orbital period and boxcar-smoothed, giving a reconstruction of the stray-light waveform during that time interval. This waveform was then subtracted from the observed magnitudes.

The upper panel of Figure 1 shows the final time series, and the lower two panels show the data after folding with the Dawson & Fabrycky (2010) ephemeris. A dip is observed at nearly zero phase, where the transit signal would be expected. In addition, a gradual rise in flux is observed away from zero phase, which is evident in the middle panel, and which has been subtracted in the lower panel based on the model described in § 3.

We emphasize that the signal shown in Figure 1 is not the outcome of a period search: the data were phased with the *predicted* ephemeris. Nevertheless, when a period search is performed the strongest signal is at 0.74 d, as shown in Figure 2. The signal has the predicted period, and the observed epoch is bracketed by the two predicted epochs of Dawson & Fabrycky (2010). It is 37 min later than the circular-orbit

prediction and 21 min earlier than the eccentric-orbit prediction. Furthermore the depth and duration of the signal conform with expectations (see § 3). With close matches to four predicted parameters (period, phase, depth, and duration) we consider the existence of transits to be established.

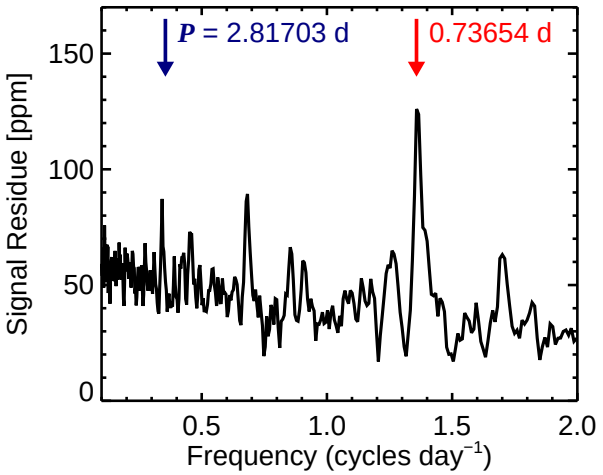

FIG. 2.— **Box-fitting Least Squares frequency spectrum of the *MOST* data.** The spectrum was computed with the method of Kovács et al. (2002). Positive peaks indicate detections of candidate transit signals with durations consistent with a near-equatorial transit of 55 Cnc.

3. ANALYSIS

3.1. *Light curve fitting*

A transit model was fitted to the light curve based on the formulas of Mandel & Agol (2002), and the Monte Carlo Markov Chain (MCMC) code of Holman et al. (2006) and Winn et al. (2007). The orbit was assumed to be circular, and the stellar limb-darkening law was assumed to be quadratic. To model the out-of-transit variation seen in the middle panel of Figure 1, we added a term

$$F_{\rm pha} = \frac{\epsilon_{\rm pha}}{2}(1-\cos 2\pi\phi), \qquad (1)$$

where ϕ is the orbital phase relative to midtransit. For completeness the model also included an occultation at $\phi = 0.5$, although occultations were not detected. The model parameters were the planet-to-star radius ratio $R_p/R_\star$, star-to-orbit radius ratio $R_\star/a$, orbital inclination i, time of midtransit T_c, amplitude of the orbital phase modulation $\epsilon_{\rm pha}$, occultation depth $\epsilon_{\rm occ}$, flux normalization (taken to be the flux just outside of transit), and limb-darkening coefficients u_1 and u_2.

Uniform priors were adopted for $R_p/R_\star$, $\cos i$, T_c, $\epsilon_{\rm pha}$, $\epsilon_{\rm occ}$ and the flux normalization. We used Gaussian priors on the stellar radius and mass, $R_\star = 0.943 \pm 0.010\ R_\odot$ and $M_\star = 0.963^{+0.051}_{-0.029}\ M_\odot$, which together act as a prior on $R_\star/a$. The radius prior is based on the interferometrically measured stellar radius (von Braun et al. 2011), and the mass prior is based on the analysis of the stellar spectroscopic properties by Takeda et al. (2007). Priors on the limb-darkening coefficients were based on theoretical values $u_1 = 0.657$ and $u_2 = 0.115$, obtained by integrating a Kurucz model with effective temperature 5327 K and $\log g = 4.48$ over the *MOST* bandpass. The sum u_1+u_2 was subject to a Gaussian prior with dispersion 0.1, and the difference u_1-u_2 (which has a negligible effect) was held fixed at the theoretical value.

The likelihood was taken to be $\exp(-\chi^2/2)$ with the usual sum-of-squares definition of χ^2. The 1σ uncertainty in each data point was taken to be the root-mean-square (rms) out-of-transit flux multiplied by a factor β intended to take into account the time-correlated noise. The factor β is the ratio between the standard deviation of residuals binned to 15 min, and the standard deviation one would expect based on the unbinned data assuming white noise (see, e.g., Pont et al. 2006, Carter & Winn 2009). The rms and β values were 101 ppm and 1.3, respectively. Table 1 gives the results.

3.2. *Signal-injection tests*

To further investigate the effects of the correlated noise and stray-light removal algorithms on the fitted transit parameters, we injected and recovered fake transit signals. Beginning with the aperture photometry, we subtracted the best-fitting transit model and added a fake signal with a different period and transit time. The fake signal had the same transit depth, duration (in phase units), $\epsilon_{\rm pha}$ and $\epsilon_{\rm occ}$ as the best-fitting model. Then, we processed the data just as was done with the undoctored data. This was repeated for 10^3 randomly chosen periods within 50% of the true period.

The recovered values of the transit and occultation depths had a scatter of 47 ppm, in excess of the statistical error of 15 ppm, and were systematically smaller by 1.9% than the injected depths. The fitted orbital phase modulations had a scatter of 68 ppm, in excess of the statistical error of 15 ppm, and the amplitudes were 6.4% smaller than the injected values. Table 1 reports the values after correcting for these biases and increased dispersions.

4. DISCUSSION

4.1. *Comparison to theoretical models*

Both the mass and radius of 55 Cnc e are known to within 10%, providing a valuable example with which to test theoretical models of super-Earth structure. To provide a broad view, the left panel of Figure 3 shows the masses and radii of the transiting exoplanets, along with theoretical curves taken from Seager et al. (2007) for "mathematicians' planets" composed of pure hydrogen, water, rock ($MgSiO_3$ perovskite) and iron. The right panel focuses on the super-Earths and shows the contours of constant mean density, along with some theoretical curves based on more detailed models.

55 Cnc e falls between the rock and water lines, suggesting it is neither a gaseous planet, nor is it simply a scaled-up terrestrial planet. Although the mean density of 55 Cnc e is similar to that of Earth, the greater compression of the interior of 55 Cnc e implies that it has a different composition. The *uncompressed* density of 55 Cnc e would be smaller than that of Earth, implying that any rock and iron must be accompanied by water, gas, or other light elements.

The right panel of Figure 3 also shows that the known super-Earths span a factor of 20 in mean density, implying a correspondingly large range of possibilities for composition and internal structure. A striking contrast exists between 55 Cnc e and Kepler-11e, which have similar masses but densities differing by a factor of 10.

4.2. *Atmosphere and orbital phase modulation*

Any atmosphere around 55 Cnc e would be strongly heated, as the planet is located less than 4 $R_\star$ from its host star.

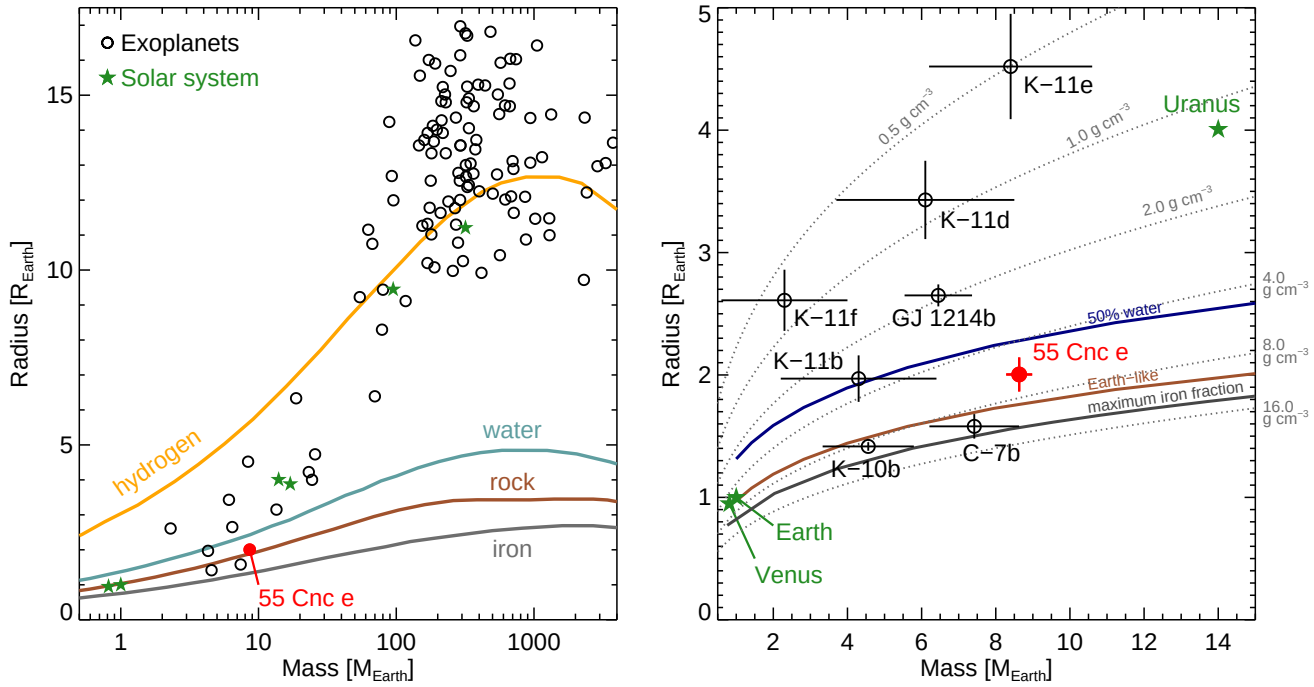

FIG. 3.— **Masses and radii of transiting exoplanets.** Open circles are previously known transiting planets. The filled circle is 55 Cnc e. The stars are Solar System planets, for comparison. *Left.*—Broad view, with curves showing mass-radius relations for pure hydrogen, water ice, rock ($MgSiO_3$ perovskite) and iron, from Figure 4 of Seager et al. (2007). *Right.*—Focus on super-Earths, showing contours of constant mean density and a few illustrative theoretical models: a "water-world" composition with 50% water, 44% silicate mantle and 6% iron core; a nominal "Earth-like" composition with terrestrial iron/silicon ratio and no volatiles (Valencia et al. 2006, Li & Sasselov, submitted); and the maximum mantle stripping limit (maximum iron fraction, minimum radius) computed by Marcus et al. (2010). Data were taken from Lissauer et al. (2011) for Kepler-11, Batalha et al. (2011) for Kepler-10b, Charbonneau et al. (2009) for GJ 1214b, and Hatzes et al. (2011) for Corot-7b. We note the mass of Corot-7b is disputed (Pont et al. 2011).

The planetary temperature at the substellar point would be $T_\star\sqrt{R_\star/a} \approx 2800$ K if the planet has a low albedo, its rotation is synchronized with its orbit and the incoming heat is reradiated locally. If instead the heat is redistributed evenly over the planet's surface, the zero-albedo equilibrium temperature is $T_\star\sqrt{R_\star/2a} \approx 1980$ K.

Atmospheres of transiting planets can be studied through occultations and orbital phase variations (see, e.g., Knutson et al. 2007). Our analysis did not reveal occultations ($\epsilon_{\rm occ} = 48 \pm 52$ ppm), but did reveal a phase modulation ($\epsilon_{\rm pha} = 168 \pm 70$ ppm). However, we cannot attribute the modulation to the changing illuminated fraction of 55 Cnc e, for two reasons. Firstly, the occultation depth is smaller than the full range of the sinusoidal modulation. Secondly, the amplitude of the modulation is too large. Reflected starlight would cause a signal no larger than $(R_p/a)^2 \approx 29$ ppm. The planet's thermal emission would produce a signal $\approx (R_p/R_\star)^2 (T_p/T_\star)^4 \approx 28$ ppm for bolometric observations, and only 5 ppm for observations in the *MOST* bandpass, even for a 2800 K planet.

One possible explanation is that the star's planet-facing hemisphere is fainter by a fraction $\epsilon_{\rm pha}$ than the other hemisphere, due to star-planet interactions. The planet may induce a patch of enhanced magnetic activity, as is the case for τ Boo b (Walker et al. 2008). In this case, though, the planet-induced disturbance would need to be a traveling wave, because the stellar rotation is not synchronized with the orbit. Fischer et al. (2008) estimated the rotation period to be 42.7 ± 2.5 d, and Valenti & Fischer (2005) found the projected rotation speed to be 2.4 ± 0.5 km s^{-1}, much slower than the synchronous value of 65 km s^{-1}.

Hence, the interpretation of the phase modulation is unclear. The power spectral density of the photometric data also displays the low-frequency envelope characteristic of stellar activity and granulation, which complicates the interpretation of gradual variations at the orbital period of 55 Cnc e. Confirming or refuting this candidate orbital phase modulation is a priority for future work.

4.3. *Orbital coplanarity*

55 Cnc e is the innermost planet in a system of at least five planets. If the orbits are coplanar and sufficiently close to 90° inclination, then multiple planets would transit. Transits of b and c were ruled out by Fischer et al. (2008).[11] However, the nondetections do not lead to constraints on mutual inclinations. Given the measured inclination for planet e of 90.0 ± 3.8 deg, the other planets could have orbits perfectly aligned with that of planet e and still fail to transit.

McArthur et al. (2004) reported an orbital inclination of $53° \pm 6.8°$ for the outermost planet d, based on a preliminary investigation of *Hubble Space Telescope* astrometry. This would imply a strong misalignment between the orbits of d and e. However, the authors noted that the astrometric dataset spanned only a limited arc of the planet's orbit, and no final re-

[11] Our *MOST* observations might have led to firmer results for planet b, since it spanned a full orbit of that planet, but unfortunately no useful data were obtained during the transit window (see Fig. 1). The *MOST* observation did not coincide with any transit windows for planets c-f.

sults have been announced. Additional astrometric measurements and analysis are warranted.

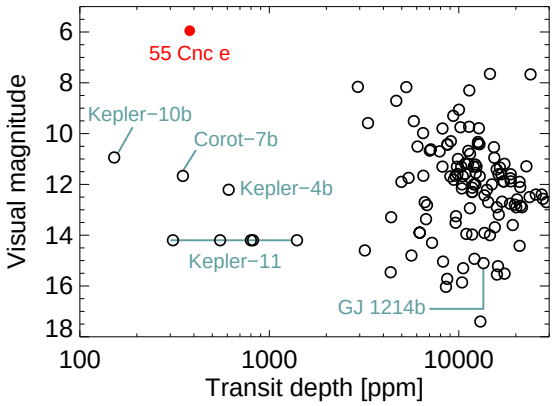

FIG. 4.— **Stellar brightness and transit depths.** The V band magnitudes and transit depths of the transiting planets with known masses and radii. Super-Earths ($M_p \lesssim 10\ M_\oplus$) are labeled.

4.4. *Potential for follow-up observations*

Figure 4 shows the stellar brightness and transit depth for each of the known transiting planets. 55 Cnc is a uniquely bright host star, towering above the other super-Earth hosts and nearly 2 mag brighter than any other transit star. However, Figure 4 also shows that the transit depth for 55 Cnc e is among the smallest known. This combination of factors causes the follow-up landscape for 55 Cnc e to differ from that of other planets.

The shallow depth will make certain follow-up observations challenging despite the abundance of photons. To resolve the transit ingress and egress, and thereby improve estimates of the planet's orbital inclination and absolute dimensions, it will be necessary to improve the signal-to-noise ratio in the phased light curve by observing more transits or using a larger-aperture telescope. More data are also needed to check on the candidate orbital phase modulation, and study the atmosphere through occultation spectroscopy. Apart from Kepler-10b, for which phase modulation was also tentatively detected (Batalha et al. 2011), these effects have not yet been seen for super-Earths.

Transit timing constraints on the system's architecture will not be easily obtained, given the shallow transit and the small amplitudes of the predicted signals. Even planet b, the nearest planet to e, is expected to perturb e's transit epoch by less than 1 s over the course of its 14 d period. The most readily detectable effect may be the Römer delay due to planet d, which should cause a sinusoidal variation in planet e's transit epoch with peak-to-trough amplitude of 24 s and period 5191 d.

On the other hand, follow-up observations of the star itself will continue to be rewarding. Already the parallax and angular diameter of the star have been measured, the stellar variability has been tracked for 11 years (Fischer et al. 2008), and there is potential for the detection of p-mode oscillations that would help define the stellar properties (see, e.g., Gilliland et al. 2011, Nutzman et al. 2011). The brightness of the star has already enabled the discovery of 4 other planets in the system, and continued monitoring has a greater potential to reveal additional bodies than is the case for fainter stars.

Finally, there is some pleasure in being able to point to a naked-eye star and know the mass and radius of one of its planets.

We thank Laura McKnight and Andrew Howard for thought-provoking conversations. Many people provided helpful feedback on this work, including Simon Albrecht, Sarah Ballard, Rory Barnes, Jacob Bean, Heather Knutson, David Latham, Barbara McArthur, Frederic Pont, Daniel Rouan, Sara Seager, and the anonymous referee. We are grateful to Kaspar von Braun for communicating the results of his team's CHARA measurement prior to publication.

J.M., D.G., A.M., and S.R. thank NSERC (Canada) for financial support. T.K. is supported by a contract to the Canadian Space Agency. R.K. and W.W. were supported by the Austrian Science Fund. D.D. is supported by a FQRNT scholarship. R.D. is supported by a National Science Foundation Graduate Research Fellowship, and D.C.F. by NASA Hubble Fellowship HF-51272.01-A. M.H. and J.W. were supported by NASA Origins award NNX09AB33G.

REFERENCES

Batalha, N. M., et al. 2011, ApJ, 729, 27
Butler, R. P., Marcy, G. W., Williams, E., Hauser, H., & Shirts, P. 1997, ApJ, 474, L115
Carter, J. A., & Winn, J. N. 2009, ApJ, 704, 51
Charbonneau, D., et al. 2009, Nature, 462, 891
Dawson, R. I., & Fabrycky, D. C. 2010, ApJ, 722, 937
Demory, B., et al. 2011, A&A, submitted [arXiv:1105.0415]
Fischer, D. A., et al. 2008, ApJ, 675, 790
Gilliland, R. L., McCullough, P. R., Nelan, E. P., Brown, T. M., Charbonneau, D., Nutzman, P., Christensen-Dalsgaard, J., & Kjeldsen, H. 2011, ApJ, 726, 2
Hatzes, A. P., et al. 2011, ApJ, submitted [arXiv:1105.3372]
Holman, M. J., et al. 2006, ApJ, 652, 1715
Knutson, H. A., et al. 2007, Nature, 447, 183
Kovács, G., Zucker, S., & Mazeh, T. 2002, A&A, 391, 369
Lissauer, J. J., et al. 2011, Nature, 470, 53
Lovis, C., et al. 2011, A&A, 528, A112
Mandel, K., & Agol, E. 2002, ApJ, 580, L171
Marcus, R. A., Sasselov, D., Hernquist, L., & Stewart, S. T. 2010, ApJ, 712, L73
Marcy, G. W., Butler, R. P., Fischer, D. A., Laughlin, G., Vogt, S. S., Henry, G. W., & Pourbaix, D. 2002, ApJ, 581, 1375
Matthews, J. M., Kusching, R., Guenther, D. B., Walker, G. A. H., Moffat, A. F. J., Rucinski, S. M., Sasselov, D., & Weiss, W. W. 2004, Nature, 430, 51
McArthur, B. E., et al. 2004, ApJ, 614, L81
Mugrauer, M., Neuhäuser, R., Mazeh, T., Guenther, E., Fernández, M., & Broeg, C. 2006, Astronomische Nachrichten, 327, 321
Novak, G. S., Lai, D., & Lin, D. N. C. 2003, Scientific Frontiers in Research on Extrasolar Planets, 294, 177
Nutzman, P., et al. 2011, ApJ, 726, 3
Pont, F., Zucker, S., & Queloz, D. 2006, MNRAS, 373, 231
Pont, F., Aigrain, S., & Zucker, S. 2011, MNRAS, 411, 1953
Rucinski, S. M., et al. 2004, PASP, 116, 1093
Seager, S., Kuchner, M., Hier-Majumder, C. A., & Militzer, B. 2007, ApJ, 669, 1279
Takeda, G., Ford, E. B., Sills, A., Rasio, F. A., Fischer, D. A., & Valenti, J. A. 2007, ApJS, 168, 297
Valenti, J. A., & Fischer, D. A. 2005, ApJS, 159, 141
von Braun, K., et al. 2011, ApJ Letters, submitted
Walker, G., et al. 2003, PASP, 115, 1023

TABLE 1
SYSTEM PARAMETERS FOR 55 Cnc e

Parameter	Value
Transit epoch [HJD]	$2,455,607.05562 \pm 0.00087$
Transit depth, $(R_p/R_\star)^2$ [ppm]	380 ± 52
Transit duration, first to fourth contact [d]	0.0658 ± 0.0013
Transit ingress or egress duration [d]	0.00134 ± 0.00011
Planet-to-star radius ratio, $R_p/R_\star$	0.0195 ± 0.0013
Transit impact parameter	0.00 ± 0.24
Orbital inclination, i [deg]	90.0 ± 3.8
Fractional stellar radius, $R_\star/a$	0.2769 ± 0.0043
Fractional planetary radius, R_p/a	0.00539 ± 0.00038
Orbital distance, a [AU]	0.01583 ± 0.00020
Amplitude of orbital phase modulation, $\epsilon_{\rm pha}$ [ppm]	168 ± 70
Occultation depth, $\epsilon_{\rm occ}$ [ppm]	48 ± 52
Planetary mass [$M_\oplus$]	8.63 ± 0.35
Planetary radius [$R_\oplus$]	2.00 ± 0.14
Planetary mean density [g cm^{-3}]	$5.9 \pm ^{1.5}_{1.1}$
Planetary surface gravity [m s^{-2}]	$21.1 \pm ^{3.5}_{2.7}$

NOTE. — These parameters were determined by fitting the *MOST* light curve as described in the text, in combination with external constraints on the orbital period $P = 0.7365400 \pm 0.0000030$ d and stellar reflex velocity $K_\star = 6.1 \pm 0.2$ m s^{-1} (Dawson & Fabrycky 2010), stellar mass $M_\star = 0.963^{+0.051}_{-0.029}\ M_\odot$ (Takeda et al. 2007), and stellar radius $R_\star = 0.943 \pm 0.010\ R_\odot$ (von Braun et al. 2011). We further assumed the orbital eccentricity to be zero, and the limb-darkening law to be quadratic with coefficients u_1 and u_2 such that $u_1 - u_2 = 0.542$ and $u_1 + u_2 = 0.772 \pm 0.100$.

Walker, G. A. H., et al. 2008, A&A, 482, 691
Winn, J. N., Holman, M. J., & Roussanova, A. 2007, ApJ, 657, 1098
Winn, J. N. 2010, in *Exoplanets*, ed. S. Seager (Tucson: University of Arizona Press) [arXiv:1001.2010]
Wisdom, J. 2005, Bulletin of the American Astronomical Society, 37, 525